Pergamon

Int. J. Multiphase Flow Vol. 23, No. 6, pp. 1085–1109, 1997

Printed in Great Britain

PII: S0301-9322(97)00030-X

0301-9322/97 $17.00 + 0.00

INVESTIGATION OF THE WALL SHEAR STRESS IN VERTICAL BUBBLY FLOW UNDER DIFFERENT BUBBLE SIZE CONDITIONS

TAY-JIAN LIU

Thermohydraulic Laboratory, Nuclear Engineering Division, Institute of Nuclear Energy Research, P.O. Box 3-3, Lung-Tan 325, Taiwan, Republic of China

(Received 7 May 1993; in revised form 15 April 1977)

Abstract—New results of experimental investigation accounted for the parametric effects of the bubble size and the two-phase flow rates on the wall shear stress are reported. The mean and the time-varying fluctuation properties of the wall shear stress are measured based on a flush-mounted hot film sensor for air–water bubbly flow in a vertical channel. The unique feature of this study is that the experiments were carried out under various fixed gas and liquid fluxes, with only the bubble size being changed at the flow entrance. This has been made by using a special bubble generator to decouple the bubble size effect from the inlet condition. The test conditions cover both the wall and core peaking void distributions of bubbly two-phase flow. It is found that the wall shear stress is strongly influenced by the internal and wall proximity structure of the flow, while both the liquid phase velocity and the wall concentrated bubbles are the dominant parameters on both the magnitude and the fluctuation intensity of the wall shear stress in the regime of bubbly flow. The present data are extensively compared with some other data sources and with the models used in predicting the wall shear stress. Due to no obvious existing wall shear stress data and models were accounted for the change in bubble size systematically, the present data thus may serve as a relatively complete comparative basis for the development of theoretical models. © 1997 Elsevier Science Ltd.

Key Words: wall shear stress, bubble size, hot film anemometer, void fraction, spectral analysis, bubbly flow

1. INTRODUCTION

The wall shear stress, τ_w, is a crucial parameter for determining the transport of momentum and energy in two-phase flow system. And wall proximity turbulence shear stress properties play a dominant role in understanding the internal structure of two-phase flow, since it is characterized by the greatest liquid velocity gradient and the highest value of turbulent fluctuations. The existing two-phase flow wall shear stress data in bubbly flow is very limited although it has been extensively applied in modern technology, such as nuclear reactor, chemical and petroleum industry, heat exchanger, and electronic cooling. In order to clarify the mechanisms of two-phase bubbly flow, it is particularly important to know the bubbles behavior in flowing liquid. Sekoguchi *et al.* (1974) observed that the motion of the isolated bubbles appeared to be related to bubble distortion, the location of the injection point, and the mean liquid flow velocity. Significantly, they found that only the distorted ellipsoidal bubbles smaller than about 5 mm in length of the major axis (d_{bl}) go along the wall for upflows, while all spherical bubbles and distorted ellipsoidal bubbles with d_{bl} larger than 5 mm rise in the core of the flow. Zun and Malahovsky (1982) observed that the trajectory of ellipsoidal bubbles movement through quiescent liquid rise up like wounding round or helix. Serizawa *et al.* (1975) and Herringe and Davis (1976) using the resistivity probe to measure the detail structure developing parameters, such as the distribution of void fraction, bubble velocity and other parameters, provided the impetus for further internal flow structure studies. Sekoguchi *et al.* (1979) further classified the vertical bubbly flow into three basic flow configurations, namely, sliding bubble, centrally coring bubble, and intermediately coring bubble. They found that these variations of void fraction profile were affected not only by the direction and velocity of the water stream, but also by the size of the bubble. Moursali *et al.* (1995) indicated that the wall void peaking

phenomena is partly due to the deceleration of the bubbles close to the wall. It also involves an actual migration of the bubbles from the external flow to the wall which is however not systematic since it is strongly size dependent. The results of similar experiments by Valukina *et al.* (1979), Kariyosaki (1985), Zun (1987) and Matsui (1988) also indicated that bubble size and shape play an important role in lateral void distribution. Recently, Serizawa and Kataoka (1987) further enlightened the physical picture of local flow field in bubbly flow as a triangular linkage among void distribution mechanism, turbulence and interfacial structures. The close linkage among these three structures is very sensitive to bubble shape and bubble size distribution. They emphasized that the bubble size effect becomes one of the most important problems to be solved in clarifying the bubbly flow structure. Lahey (1988) also indicated that the models which are to be valid over a wide range of conditions should include the effect of bubble size.

Several experimental studies (Davis 1974; Herringe and Davis 1978; Nakoryakov *et al.*, 1981; Sato *et al.*, 1981; Avdeev 1984) appeared in the literature on the flow of gas-liquid mixtures in vertical pipes, which have qualitatively addressed the influence of bubble diameter and/or phase distribution effect on the wall shear stress. However, the wall boundary region under well-controlled inlet bubble size flow conditions has not yet been investigated systematically in a vertical pipe flow. Davis (1974) and Herringe and Davis (1978) account for the effects of phase and velocity distributions on friction factors. They concluded that for bubbly flows, the inclusion of these distribution effects did not substantially alter friction estimates which are approximately 10% above the single-phase values. Thus a correlation of friction factor monotonous increase of area-averaged void fraction was given. Recently, Marie *et al.* (1991) investigated the effects of bubbles on both the turbulent and the kinematic structures of a boundary layer on a flat plate. They found that wall shear stress increase with the magnitude of void fraction peak in the wall region which is consistent with the model proposed by Marie (1987). Nakoryakov *et al.* (1981) used the electrochemical method to measure the wall shear stress in an upward bubbly and slug flow regimes. Their data revealed that the flow in a bubbly flow regime with $J_L \leqslant 1$ m/s is of the hysteresis type and the existence of two stable bubbly flow regimes is possible. This non-uniqueness of the wall shear stress characteristics under the same J_L and J_G conditions also was reported by Sato *et al.* (1981) and Avdeev (1984).

Nowadays, it has been made clear through several recent works (Serizawa *et al.*, 1988, 1991; Liu 1991, 1993, 1994; Liu and Bankoff 1993a, b) that the bubble lateral migration and flow regime transition are very sensitive to the variation in bubble size and bubble coalescence effect during the development of the bubbly flow. It is found that performing experiment under identical gross flow condition with different sizes of bubble generated at inlet, in which several important local hydraulic characteristics such as void distribution; bubble size and its number distributions; interfacial area concentration; etc. might be different. This bubble size effect might also be one of the important reasons for the discrepancies existing among published data on wall shear stress and on other local internal parameters determined through different experiments.

Very few experiments in studying the effect of bubble size have been conducted by using different bubble generators. However, under fixed gas and liquid flow rates, the bubble size from these kinds of bubble generators cannot be controlled by the experimenter; this limitation makes it very hard to elucidate the parametric effect. In addition, the use of different bubble generators has inevitably mixed the effect of the inlet flow condition with the effect of bubble size. Serizawa and Kataoka (1987) first claimed the importance of the effect of different bubble generator designs on local void fraction distribution. To understand the bubble size effect specifically, it is quite necessary to use a single bubble generator to perform experiments for generating different sizes of bubble at the inlet under various fixed gas and liquid flow rate conditions. The pioneering study of Serizawa *et al.* (1988) used a specially designed bubble generator to change the bubble size at the test section entrance under the same combination of two phase flow rates, in which the bubble size was carefully controlled and identified. A similar bubble generator which was a slight modification of Serizawa's design, has been used by Liu (1991, 1993, 1994) in studying the phase distribution phenomena, with particular emphasis on the effects of the bubble size and axial length from the entrance on the behavior of structural development under well-controlled inlet bubble size flow conditions.

The objective of the present study is to account for the effects of bubble size on the behavior of turbulent shear stress in the wall vicinity. New results of wall shear stress and the intensity of

turbulent fluctuations are presented for air–water bubbly flow in a vertical channel. An indirect method of using a flush-mounted hot film probe was utilized. The excellent frequency response of this kind of probe makes it possible in sensing the time-varying properties of the wall shear stress faithfully. This paper summarizes the experimental results on the time-varying fluctuation properties and the contribution of bubble size and phase distribution as well as the flow rates of the two phases to wall shear stress. Finally, the present data are compared with some other data sources and with the existing models used in predicting the wall shear stress.

2. EXPERIMENTAL APPARATUS

Experiments were carried out for vertical upward bubbly flow in a circular pipe using filtered air and demineralized water as the working fluid. The test section was made of an 8 m long, smooth and transparent Lexan tube, with i.d. = 57.2 mm. The two-phase flow was realized by separately supplied and controlled flow rates of air and water through a bubble generator and then mixed in the test section. Schematic diagram of the experimental facility is shown in figure 1.

A special bubble generator (figure 2), same as that previously applied by Liu (1991, 1993), was used to change the bubble size as desired for a given combination of gas and liquid volumetric fluxes. Air was injected into the water flow through a sintered cylinder of 7 μm nominal porosity, located at the center of the air chamber, and was sheared away by a high speed nozzle water jet (J_j) with velocities up to 10 m/s. Here, J_j is defined as the volumetric flux of water flow through the bubble injector with i.d. = 9.7 mm, while J_L and J_G are the volumetric fluxes of water and air

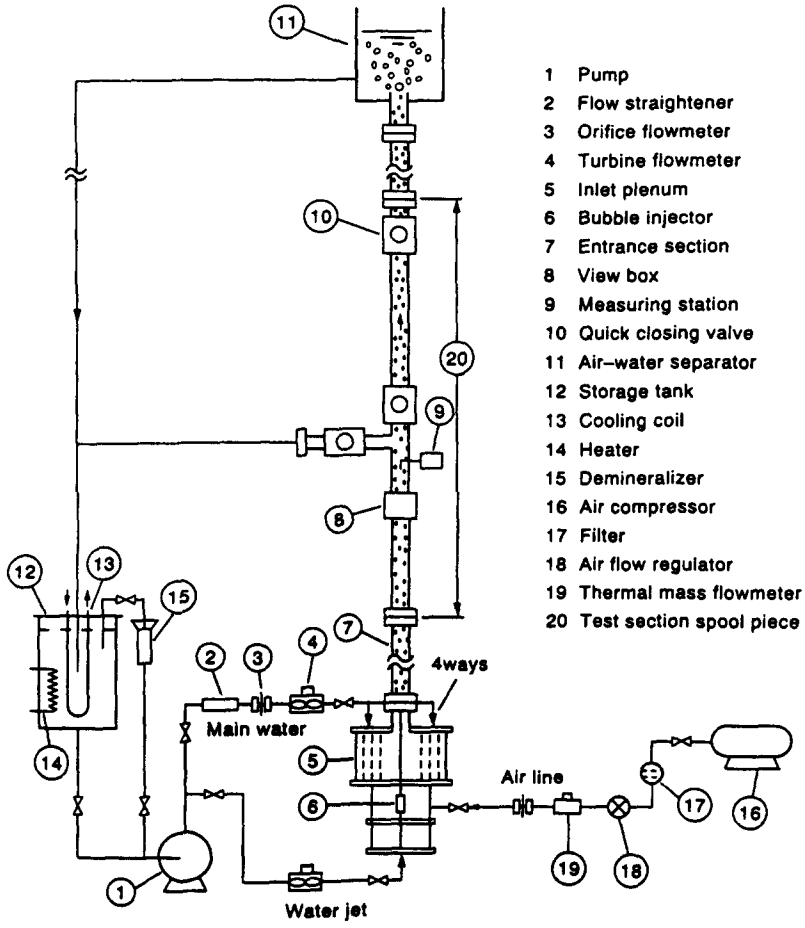

Figure 1. Schematic diagram of the experimental facility.

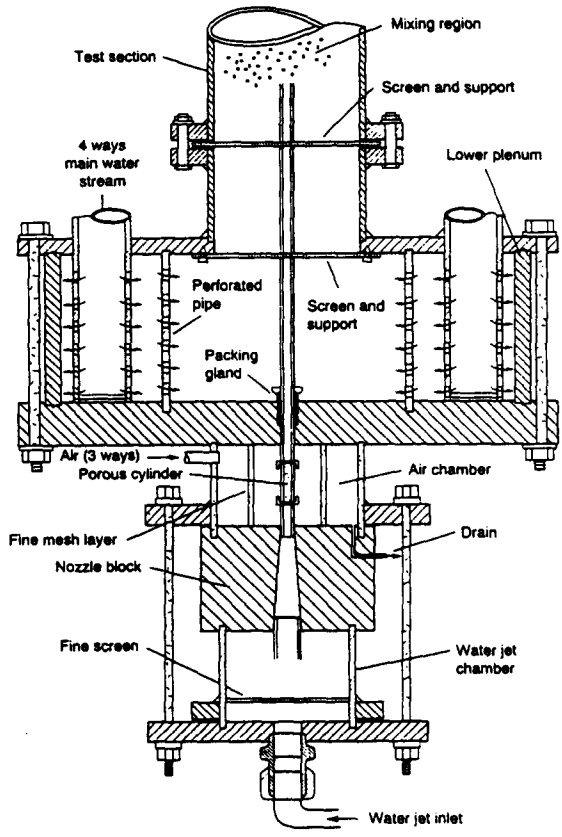

Figure 2. Test section inlet plenum and bubble generator.

flow through the test section, respectively. Thus, a wide range of initial bubble size from <1 to 20 mm in diameter can be generated by setting the jet velocity at an appropriate value.

To stabilize the resultant inlet flow field and to eliminate secondary effects, the mixing quality of the main liquid stream with the two-phase jet at the entrance of the test channel was significantly improved by the following arrangements.

(1) Main water stream was driven through four identical perforated sections arranged symmetrically and well mixed through a central perforated pipe in the inlet plenum. The uniformity of this upward water velocity was further improved by flowing through two layers of fine mesh screen before mixing with the two-phase jet.

(2) Air stream was driven through three symmetrical ways into the air chamber. Before entering the central porous cylinder, the air flow was through a 50 μm fine mesh layer to stabilize the airflow.

(3) Water jet flow rate in the central nozzle was stabilized by flowing through a fine screen installed at the entrance of the water jet chamber.

(4) To reduce the bubble size change resulting from secondary flow, the entrance mixing region associated with the main water stream and the outlet of bubble injector was arranged in the same direction and with the same size as that of the test channel.

Wall shear stress was measured with a hot film probe (TSI-1268W) which was cast into an acrylic mounting block and was flush-mounted on the internal surface of the test tube. Details of the probe installation is shown in figure 3. The hot film sensor was made of a thin platinum with dimensions of 1.0×0.127 mm and coated with a thin layer of quartz. It was located at $L/D = 60$ oriented with the longer side normal to the main flow direction. The square-wave test indicated that the frequency resolution of this wall shear stress probe is approximately 15 kHz. The sensor was controlled at constant temperature (46.7°C) by a hot film anemometer (TSI IFA-100) which was operated at a low overheat ratio of 1.05 in order to avoid bubble nucleation.

The flow temperature was maintained at 20 ± 0.1°C during both calibration and measurement, which was measured by a 1.5 mm o.d. sheathed in-stream bare junction thermocouple, located at 2 in downstream of the probe position. Two pairs of pressure taps oriented diametrically opposite along the center line of the test section were used to measure the pressure gradient in the same hot film probe region for double checking during calibration. Each pair of the pressure taps were connected to a Rosemount differential pressure transducer, with an accuracy of 0.1 mm water head. Due to the highly fluctuating nature in pressure gradients and anemometer output, all these signals were digitized simultaneously by an on-line data acquisition system (TSI IFA-200) with sampling rate of 5 kHz. For each bubbling condition, a total of $N = 100{,}000$ samples per channel were then used to process the shear stress result.

3. WALL SHEAR STRESS MEASUREMENT

Prior to the experiment, calibration was conducted in a series of single-phase water flow conditions for the output signals of the wall shear stress probe. A flush-mounted hot film sensor was calibrated *in situ* thereby avoiding misalignment of the sensor surface, which could drastically change the result. A well-known relationship between the instantaneous values of the anemometer output voltage (E_a) and of the wall shear stress (τ_w) was given by

$$E_a^2 = a + b \cdot \tau_w^{1/3}. \quad [1]$$

The coefficients a and b were determined by least square fitting of the mean values of shear stress (τ_w) and of bridge voltage (E_a), such as

$$\overline{E_a}^2 = a + b \cdot \overline{\tau_w}^{1/3}. \quad [1']$$

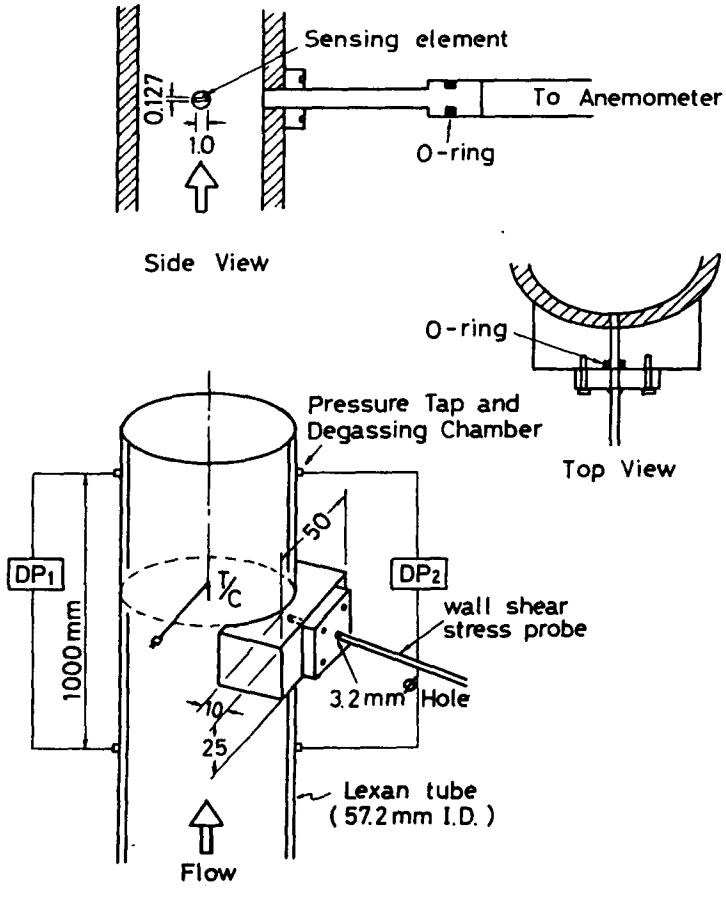

Figure 3. Wall shear stress probe installation.

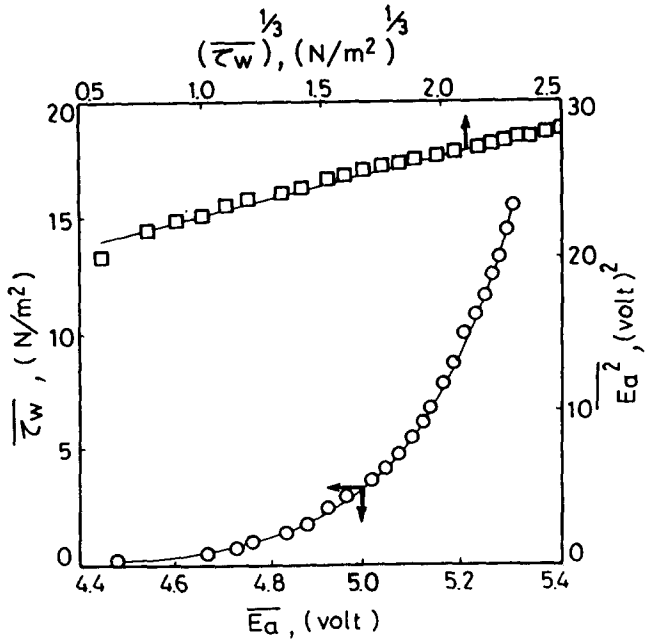

Figure 4. Calibration of wall shear stress probe.

The standard wall shear stress was obtained from [2] by measuring the pressure gradient of the single-phase water flow (dp/dz) in the same probe region, covering the Reynolds number from 10^4 to 2×10^5

$$\overline{\tau_w} = [(dp/dz) - \rho_L \cdot g] \cdot (D/4). \quad [2]$$

As shown in figure 4, the data closely followed the well-known law related to the square of the bridge voltage to one-third power of the shear stress.

The consistency of both wall shear stresses measured by hot film probe and pressure drop is $\pm 2\%$, which is within experimental uncertainty. In addition, the friction factors (f) measured by the water calibrated hot film sensor were compared with the calculated result from Karman–Prandtl friction factor correlation for turbulent flow in smooth pipes

$$1/\sqrt{f} = 2.0 \log_{10}(R_e \cdot \sqrt{f}) - 0.8, \quad [3]$$

where R_e is the Reynolds number based on the internal diameter of the test section. These comparisons indicated that both of them are in good agreement.

In a two-phase flow there is a wall liquid film which is sufficient for the wall shear stress probe operation. Therefore, as shown by Martin (1984) and Whalley and McQuillan (1985), the probe operation in single- and in two-phase flows is essentially the same. Thus, the instantaneous wall shear stress was determined from the instantaneous bridge output from [1]. The mean and the fluctuation intensity values of the shear stress can then be obtained by

$$\overline{\tau_w} = \frac{1}{N} \sum_{i=1}^{N} \tau_{w,i} \quad [4]$$

$$\sqrt{\overline{\tau_w'^2}} = \left[\frac{1}{N-1} \sum_{i=1}^{N} (\tau_{w,i} - \overline{\tau_w})^2 \right]^{1/2}. \quad [5]$$

In order to eliminate uncertainty resulting from the hot film sensor drift, the consistency of single-phase (water) flow anemometer output in two-phase run was frequently checked with the calibration data. The results of no observable drift data were used to process the wall shear stress.

In two-phase flow conditions, the wall shear stress also was calibrated from the measured pressure gradient (dp/dz) and void fraction $\langle\epsilon\rangle$ determined by hold-up method, such that

$$\overline{\tau_w} = [(dp/dz) - (1 - \langle\epsilon\rangle)\rho_L \cdot g] \cdot (D/4). \quad [6]$$

The consistency of the results obtained from [4] and from [6] was within $\pm 6.7\%$ in 90% of the test. These deviations may be attributed primarily to the inherent fluctuation of the probe output voltage (E_a) in two-phase bubbly flow, while the shear stress is proportional to the sixth power of E_a.

A series of experiments were conducted under the flow combination of four water superficial velocities (J_L: 0.5, 1.0, 2.0 and 3.0 m/s) and three air superficial velocities (J_G: 0.1, 0.2 and 0.4 m/s). For each fixed combination of J_L and J_G, the size of bubbles were changed by 5 nozzle liquid jet velocities (J_j: 0.5, 1.0, 2.0, 4.0 and 6.0 m/s). The experimental results corresponding to all these conditions are presented in table 1.

4. EXPERIMENTAL RESULTS

4.1. The development of bubble size distribution at the entrance region

In order to evaluate the performance of the bubble generator used in this study, it is essential that the mixing quality of the inlet conditions should be clearly assessed. This has been made by using a radially transversing dual-sensor resistivity probe measured at different distances from the inlet of the bubble generator. The development of bubble size distributions at the entrance region have been determined from the measured bubble chord length spectrum based on a statistical treatment of the bubble resident time. The details of the method was given in Liu and Bankoff (1993b). Typical results are presented in figures 5–7 for the two different flow conditions (a) and (b) at the three entrance lengths of $L/D = 12$, 30 and 60.

As measured from previous study (Liu 1993) the small bubbles in the inverted–conical two-phase round jet injected from the inlet of the test section will travel a characteristic mixing length where the boundary of the jet is extended to the pipe wall. The value of characteristic mixing length will depend on the flow conditions. Generally, the lower the main liquid flow rate and/or the higher the gas flow rate and/or the lower the liquid jet flow rate (i.e. the larger the bubble size), the smaller is the mixing length—due to the lateral mixing effect that outweighed the low axial inertia force of the two-phase jet. It is observed that the mixing length is smaller than $5D$ for all the flow conditions investigated.

At $L/D = 12$, most of the small bubbles were crowded at the center, resulting from a coaxial two-phase jet mixed with the upward surrounding main water stream at the inlet of the test section. At this elevation, a convex profile of void fraction and bubble frequency was attained. With further development, bubbles gradually grow and are transported from the jet core into the wall. As a result, the wall peak height of the gas content increases with the distance from the injection point and the lower the gas content in the core. It should be noted that at $L/D = 30$, a relatively larger bubble size was measured near the wall at condition (a) but a more uniform bubble size appeared at condition (b). The observed maxima near the wall in condition (a) may be due to the highly concentrated bubbles having a greater probability of bubble coalescence in a rather lower liquid flux condition. The bubble elongation in the flow direction caused by the large gradient of the shear stress distribution close to the void peaking may be another reason (Liu and Bankoff 1993a). At $L/D = 60$, the bubble sizes in both conditions are nearly uniformly distributed in the cross-section area. In this elevation, a concave profile of void fraction and bubble frequency is attained. Consequently, a continual axial cylindrical symmetry flow development along the tube could be expected, though the bubble size is increased slightly provided that the buoyancy effect is dominant as L/D increases.

From these bubble chord length spectra shown in figures 5–7, it is suggested that the decrease in sensitivity to the initial condition with increased distance from the inlet and the hydrodynamic equilibrium of vertical upward bubbly flow could be attained in a certain distance from the entrance. This can be made as the higher the main liquid flow rate and/or the lower the gas flow rate and/or the higher the liquid jet flow rate (i.e. the smaller the bubble size), the shorter is the

Table 1. Comparison of the present two-phase wall shear stress data with correlations

Run No.	Condition for $D = 57.2$ mm	Bubble J_j (m/s)	Bubble $\langle d_b \rangle$ (mm)	Void fraction $\langle \epsilon \rangle$ (%)	Void fraction ϵ_{pk} (%)	Void fraction Z_{pk}	Measured data τ_{wo} (Pa)	Measured data τ_w (Pa)	Measured data R_{exp}	Sato prediction τ_{Swo} (Pa)	Sato prediction R_{SBav}	Sato prediction R_{SB}	Model prediction R_{Mav}	Model prediction R_{Mpk}	Model prediction R_{HDv}	Model prediction R_{ANv}	Model prediction R_{Bav}
01		0.5	9.87	12.0	17.82	0.000	0.90	1.28	1.41	0.96	1.26	1.58	1.64	1.81	1.04		1.06
02	$J_L = 0.5$m/s	1.0	8.40	13.0	19.54	0.210	0.92	1.27	1.38	0.98	1.12	1.47	1.67	1.86	1.04		1.06
03	$J_G = 0.1$ m/s	2.0	4.18	15.0	20.42	0.875	0.96	2.26	2.35	1.02	1.99	2.21	1.73	1.88	1.05	1.25	1.06
04	$\beta = 16.6\%$	4.0	3.19	15.1	19.47	0.910	0.96	2.37	2.46	1.02	2.08	2.36	1.73	1.86	1.05		1.07
05		6.0	2.94	15.1	18.37	0.910	0.96	2.31	2.40	1.02	1.85	2.20	1.73	1.82	1.05		1.07
06		0.5	6.60	8.7	16.34	0.000	2.90	3.09	1.06	3.05	1.18	1.22	1.27	1.38	1.03		1.03
07	$J_L = 1.0$ m/s	1.0	6.13	9.3	13.74	0.000	2.94	3.26	1.11	3.09	1.23	1.21	1.28	1.34	1.03		1.03
08	$J_G = 0.1$ m/s	2.0	3.70	9.5	15.91	0.980	2.95	4.11	1.39	3.10	1.79	2.00	1.28	1.38	1.03	1.12	1.03
09	$\beta = 9.0\%$	4.0	3.03	10.5	22.20	0.980	3.01	5.29	1.76	3.16	2.11	2.27	1.29	1.46	1.03		1.03
10		6.0	2.81	10.6	20.32	0.980	3.02	5.30	1.76	3.17	1.99	2.17	1.30	1.44	1.03		1.03
11		0.5	9.98	14.3	23.39	0.000	3.25	3.22	1.00	3.42	1.44	1.64	1.35	1.48	1.05		1.04
12	$J_L = 1.0$ m/s	1.0	8.67	14.5	22.33	0.000	3.27	3.32	1.02	3.43	1.21	1.39	1.36	1.46	1.05		1.04
13	$J_G = 0.2$ m/s	2.0	5.01	15.7	19.87	0.000	3.35	4.81	1.44	3.52	1.75	2.03	1.37	1.43	1.05	1.25	1.04
14	$\beta = 16.6\%$	4.0	4.02	16.0	25.26	0.945	3.37	5.95	1.77	3.54	2.08	2.48	1.38	1.50	1.06		1.04
15		6.0	3.93	16.0	28.97	0.945	3.37	5.97	1.77	3.54	2.20	2.55	1.38	1.55	1.06		1.04
16		0.5	16.17	22.1	36.98	0.000	3.86	3.39	0.88	4.05	1.66	2.26	1.46	1.67	1.09		1.06
17	$J_L = 1.0$ m/s	1.0	13.36	23.0	38.68	0.000	3.94	3.39	0.86	4.13	1.52	1.84	1.47	1.69	1.09		1.06
18	$J_G = 0.4$ m/s	2.0	7.09	24.0	30.41	0.000	4.03	5.84	1.45	4.23	1.63	1.99	1.49	1.57	1.10	1.51	1.07
19	$\beta = 28.5\%$	4.0	4.96	24.5	32.00	0.910	4.08	7.26	1.78	4.28	1.91	2.35	1.49	1.60	1.10		1.07
20		6.0	4.85	25.0	32.92	0.910	4.13	7.27	1.76	4.33	2.01	2.46	1.50	1.61	1.11		1.07

Table 1—(*continued opposite*)

Table 1—*continued*

Run No.	Condition for $D = 57.2$ mm	Bubble J_j (m/s)	Bubble $\langle d_b \rangle$ (mm)	Void fraction $\langle \epsilon \rangle$ (%)	Void fraction ϵ_{pk} (%)	Void fraction Z_{pk}	Measured data τ_{wo} (Pa)	Measured data τ_w (Pa)	Measured data R_{exp}	Sato prediction τ_{Swo} (Pa)	Sato prediction R_{SBav}	Sato prediction R_{SB}	Model prediction R_{Mav}	Model prediction R_{Mpk}	Model prediction R_{HDv}	Model prediction R_{ANv}	Model prediction R_{Bav}
21		0.5	4.67	4.7	7.67	0.000	9.30	11.12	1.20	9.73	1.22	1.27	1.09	1.12	1.01		0.99
22	$J_L = 2.0$ m/s	1.0	4.36	5.1	8.76	0.000	9.37	10.99	1.17	9.80	1.16	1.20	1.10	1.13	1.01		0.99
23	$J_G = 0.1$ m/s	2.0	3.31	5.3	10.99	0.910	9.41	11.08	1.18	9.84	1.29	1.35	1.10	1.15	1.01	1.06	0.99
24	$\beta = 4.7\%$	4.0	3.09	5.7	15.30	0.945	9.48	11.59	1.22	9.91	1.48	1.58	1.10	1.18	1.02		0.99
25		6.0	2.91	5.8	19.54	0.945	9.50	11.78	1.24	9.93	1.58	1.64	1.10	1.21	1.02		0.99
26		0.5	6.24	9.5	16.66	0.000	10.21	11.16	1.09	10.67	1.25	1.37	1.14	1.19	1.03		1.00
27	$J_L = 2.0$ m/s	1.0	5.61	9.5	14.02	0.000	10.21	11.42	1.12	10.67	1.21	1.30	1.14	1.17	1.03		1.00
28	$J_G = 0.2$ m/s	2.0	4.78	9.7	12.07	0.945	10.25	11.47	1.12	10.71	1.35	1.47	1.14	1.16	1.03	1.12	1.00
29	$\beta = 9.0\%$	4.0	4.22	10.5	28.44	0.945	10.41	12.45	1.20	10.88	1.72	1.97	1.15	1.27	1.03		1.00
30		6.0	3.97	10.8	32.10	0.945	10.48	12.97	1.24	10.95	1.72	1.90	1.15	1.30	1.03		1.00
31		0.5	7.98	16.9	23.69	0.000	11.90	11.84	1.00	12.43	1.33	1.44	1.43	1.24	1.06		1.02
32	$J_L = 2.0$ m/s	1.0	6.95	17.2	29.13	0.000	11.98	11.95	1.00	12.51	1.24	1.29	1.19	1.28	1.06		1.02
33	$J_G = 0.4$ m/s	2.0	5.32	17.3	21.22	0.105	12.00	12.36	1.03	12.54	1.40	1.56	1.20	1.22	1.06	1.25	1.02
34	$\beta = 16.6\%$	4.0	4.54	18.0	38.44	0.945	12.19	14.46	1.19	12.74	1.78	2.05	1.20	1.34	1.07		1.02
35		6.0	4.21	18.0	40.32	0.945	12.19	15.43	1.27	12.74	1.77	2.02	1.20	1.35	1.07		1.02
36		0.5	2.79	2.7	4.86	0.000	17.89	18.42	1.03	19.41	1.10	1.10	1.04	1.06	1.01		1.00
37	$J_L = 3.0$ m/s	1.0	2.66	2.7	4.83	0.770	17.89	18.40	1.03	19.41	1.08	1.08	1.04	1.06	1.01		1.00
38	$J_G = 0.1$ m/s	2.0	2.52	2.8	4.78	0.875	17.93	18.60	1.04	19.45	1.12	1.13	1.04	1.06	1.01	1.04	1.00
39	$\beta = 3.2\%$	4.0	2.45	2.8	5.59	0.875	17.93	18.33	1.02	19.45	1.11	1.11	1.04	1.07	1.01		1.00
40		6.0	2.19	2.8	4.80	0.910	17.93	18.52	1.03	19.45	1.11	1.10	1.04	1.06	1.01		1.00
41		0.5	3.78	6.1	8.45	0.210	18.82	18.83	1.00	20.70	1.12	1.15	1.07	1.08	1.02		1.02
42	$J_L = 3.0$ m/s	1.0	3.62	6.1	8.54	0.840	18.82	19.29	1.03	20.70	1.13	1.15	1.07	1.08	1.02		1.02
43	$J_G = 0.2$ m/s	2.0	3.47	6.2	9.43	0.840	18.86	19.14	1.02	20.74	1.14	1.16	1.07	1.09	1.02	1.08	1.02
44	$\beta = 6.2\%$	4.0	3.11	6.2	9.33	0.840	18.86	19.20	1.02	20.74	1.18	1.20	1.07	1.09	1.02		1.02
45		6.0	3.03	6.2	9.87	0.910	18.86	18.71	0.99	20.74	1.19	1.21	1.07	1.09	1.02		1.02

distance from the entrance. More detailed result of the two-phase mixing properties in the entrance region was reported in Liu (1993), which included the detailed information about the radial profiles of void fraction, bubble size and its number density, and bubble velocity. All these experimental results reveal that the quality of the inlet condition is good enough to study the effect of bubble size on the two-phase flow structure.

4.2. *Statistical nature of the wall shear stress fluctuations*

By using [1], the instantaneous voltage outputs of shear stress probe, as sampled by high-speed data acquisition system, were converted to the corresponding instantaneous wall shear stress data. A series of time history of the temporal fluctuations of the shear stress on the wall is processed. The results of two typical conditions are illustrated in figure 8(a). The corresponding frequency spectrum and power spectral density are also presented in figure 8(b)–(c). Generally, there was a rise in the wall shear stress associated with the passage of the disturbance waves onto the thin liquid film that had immediate contact with the wall. This feature was confirmed by Martin (1984), who observed the thin liquid film in annular flow by a photochromic dye tracing visualization techniques.

The frequency spectrum was obtained by transferring the original time-varying fluctuations signal through a Fast Fourier Transform (FFT) routine to quantify the average wave amplitude as a function of frequency. These relative amplitudes of the FFT depend on the length of the original signal. For easy comparison under all conditions, the spectrum was normalized with the

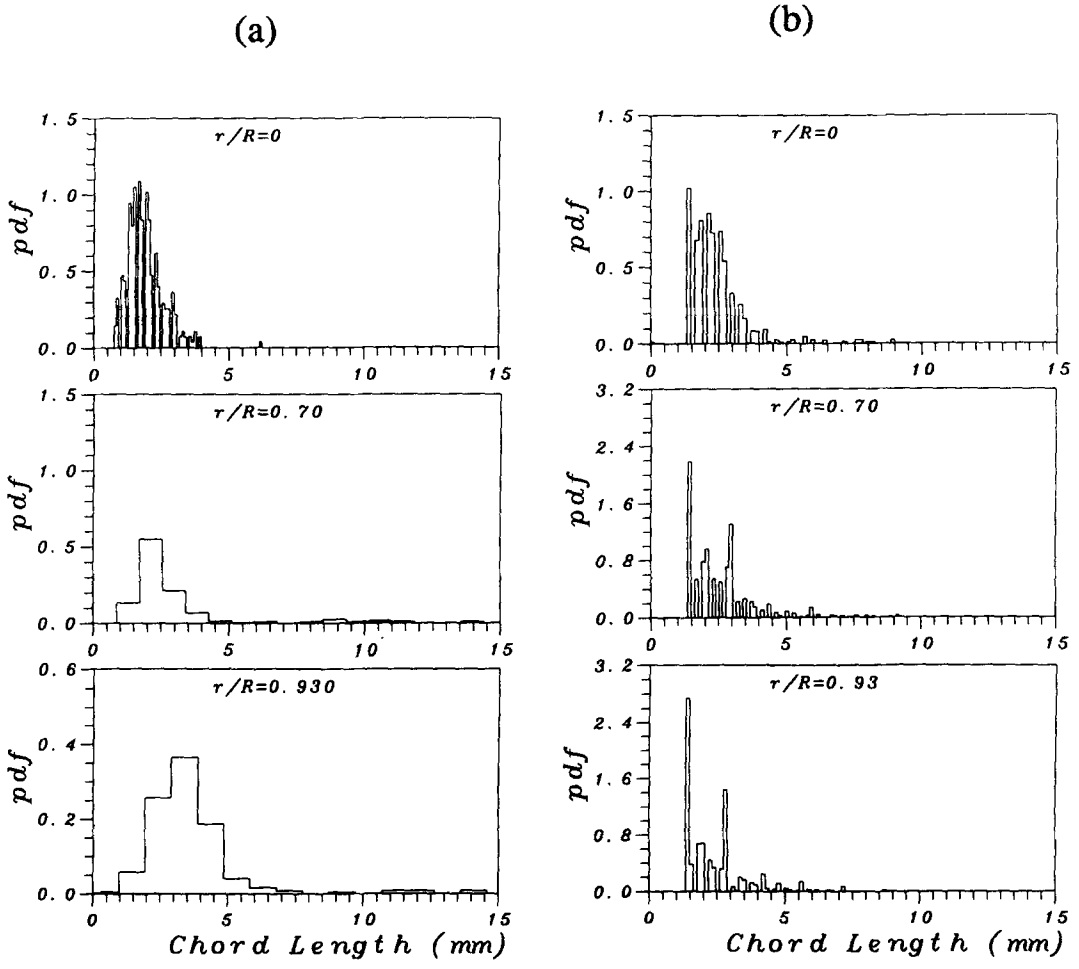

Figure 5. Bubble chord length spectrum at $L/D = 12$, under the condition of (a) $J_L = 1.0$ m/s, $J_G = 0.2$ m/s, $J_j = 4.0$ m/s; (b) $J_L = 2.0$ m/s, $J_G = 0.4$ m/s, $J_j = 4.0$ m/s.

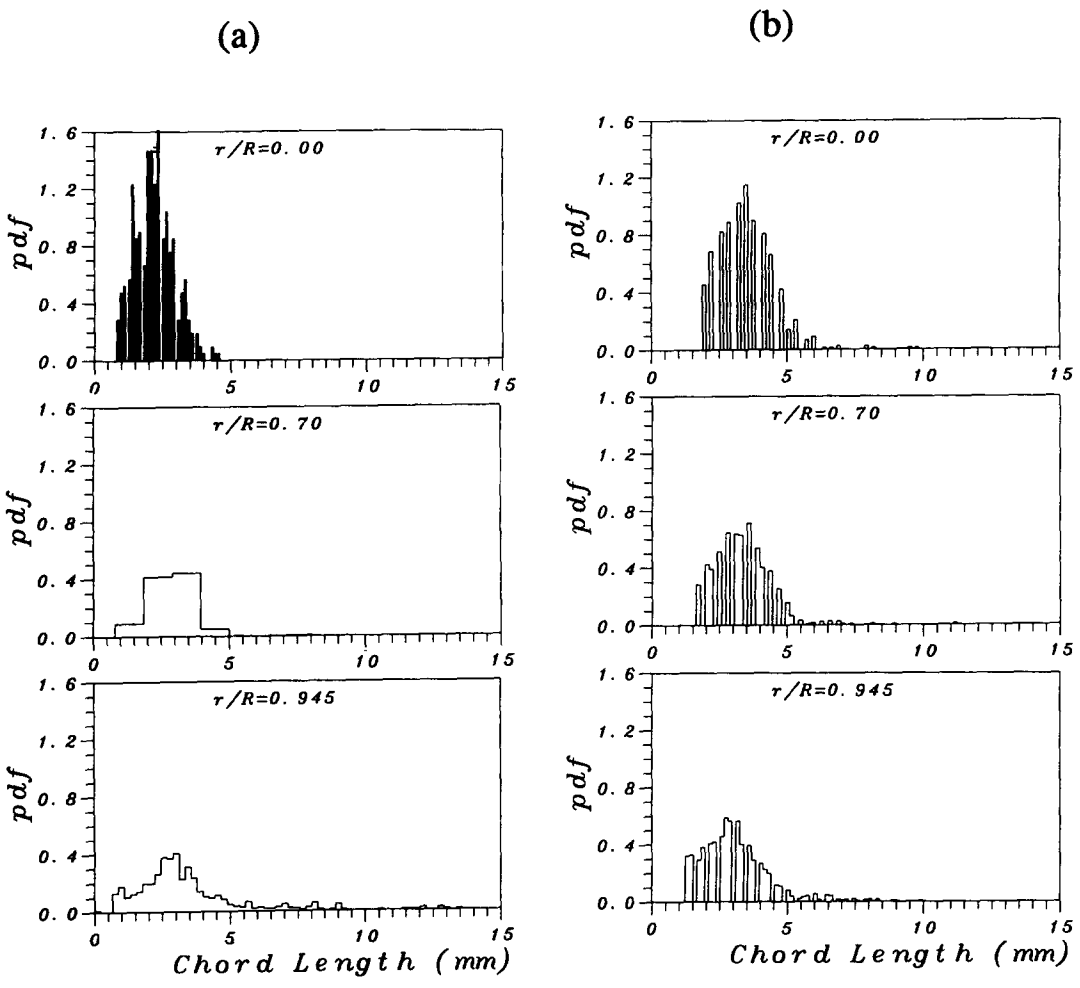

Figure 6. Bubble chord length spectrum at $L/D = 30$, under the condition of (a) $J_L = 1.0$ m/s, $J_G = 0.2$ m/s, $J_j = 40$m/s; (b) $J_L = 2.0$ m/s, $J_G = 0.4$ m/s, $J_j = 4.0$ m/s.

area covering the whole frequency domain. As illustrated in figure 8(b), the shear stress spectrum diagram in bubbly flow appears as a multi-peak amplitude in a broad frequency domain. The high-frequency and small-amplitude waves do not exhibit a dominant frequency. The frequency of large-scale pulsations ranged up to 100 Hz appears to be the major part contributed to the intensity of shear fluctuations. This prominent feature appearing in bubbly flow is substantially different from the frequency spectrum in annular flow which preserved only one single dominant frequency studied by Martin (1984).

The power spectral density (PSD) function was computed by transforming the time-series of shear stress fluctuations through the magnitude square of the first half of the FFT and the Hamming window by Welch periodogram method (Marple 1987), and finally factored out by the length of the signal. The use of Hamming window was to suppress the sidelobes in the spectral analysis. As can be seen from figure 8(c), the wall shear stress in two-phase bubbly flow preserves a fluctuating frequency much higher than the corresponding single-phase (water) flow. Introducing bubbles generally flattens the shape of the power spectrum. As more bubbles are introduced, the high frequency components increase relative to the low frequency ones. The same tendency also was found for increasing either liquid flow rate or nozzle liquid jet velocity (to decrease bubble size), provided without changing the other flow conditions, making the relative PSD weighing of high frequency portion increase.

Since the turbulence energy structure is a continuous cascade of turbulent kinetic energy transferred from the process of low to high frequencies grinding down of large eddies into smaller

ones; the higher frequency waves are capable of rapidly extinguishing the wave energy through viscous dissipation. The above-mentioned augmented high-frequency part of PSD may be one of the important reasons to promote the wall shear stress. The consistent tendency can be confirmed from the latter section that the wall shear stress and its turbulent fluctuations in bubbly flow regime are indeed, strongly dependent on the flow structure near the wall. Presumably, the shear stress is primarily due to the predominant role of multi-peak large-scale low-frequency wave components, whereas the interaction between the wall concentrated bubbles and the thin liquid film proximity to the wall outweigh the high-frequency small-scale wave components, promoted both the mean and fluctuation intensity of the wall shear stress.

4.3. *Parametric effect on the wall shear stress*

4.3.1. Two phases velocity effect. Figures 9 and 10 illustrate the effect of the liquid- and gas-superficial velocities, respectively, on the wall shear stress and its turbulent intensity. The corresponding values of single-phase water flow are also included in figure 9. It can be seen that for both of the single-phase water flow and two-phase bubbly flow, the increase of the liquid velocity highly increases the magnitude of both quantities in an almost linear rate. As expected, besides the two-phase wall shear stress being always higher than that of the single-phase one, they are parallel. However, figure 10 indicate that the increase of the gas velocity only slightly increase the τ_w and so does its fluctuations, as compared with the liquid velocity effect. As liquid velocity increased further, the differences of the τ_w among the various two-phase flow conditions would be

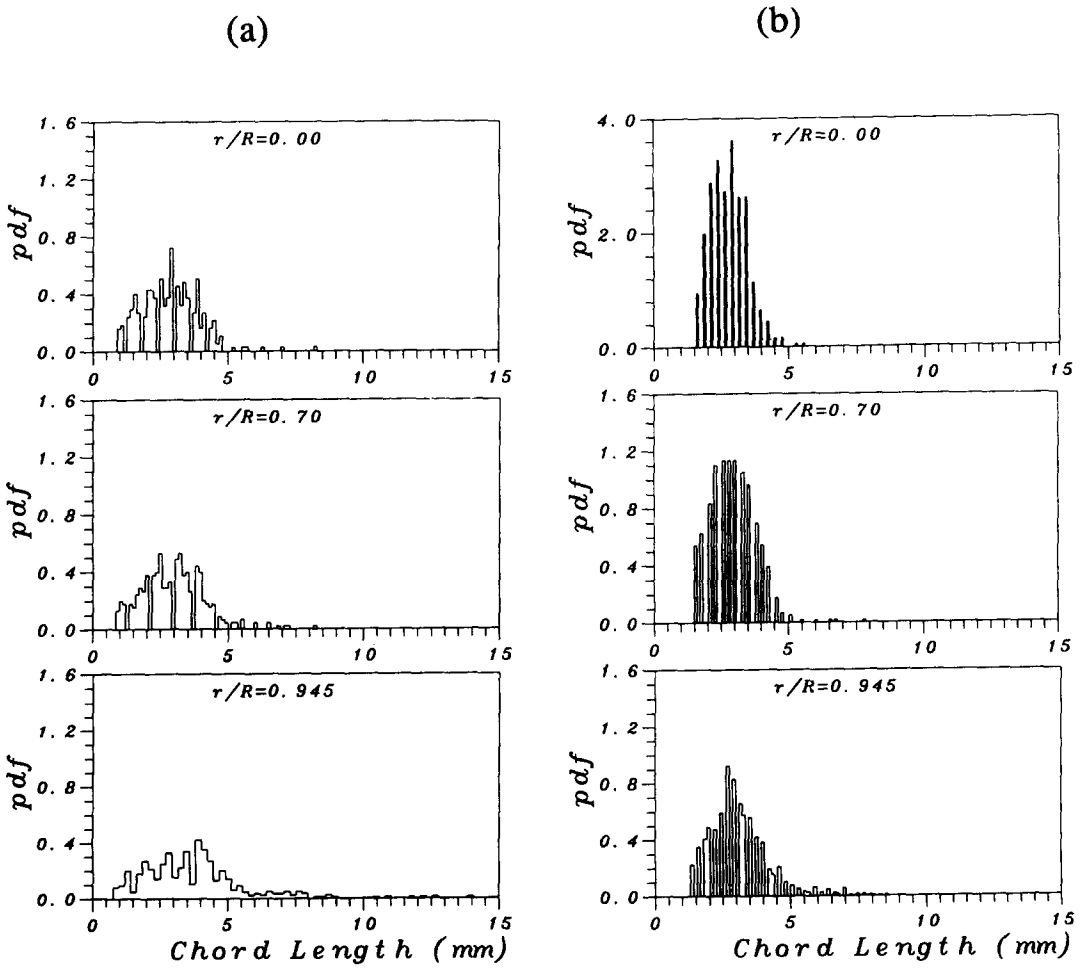

Figure 7. Bubble chord length spectrum at $L/D = 60$, under the condition of (a) $J_L = 1.0$ m/s, $J_G = 0.2$ m/s, $J_j = 4.0$ m/s; (b) $J_L = 2.0$ m/s $J_G = 0.4$ m/s $J_j = 4.0$ m/s.

diminished. Namely, as shown in table 1, $R_{exp}(=\overline{\tau_w}/\overline{\tau_{wo}})$ close to 1 at $J_L = 3.0$ m/s. $\overline{\tau_w}$ is the two-phase wall shear stress, while in here, τ_{wo} represents the single-phase wall shear stress in which the water flow would be exerted by the bulk velocity of $J_L/(1 - \langle\epsilon\rangle)$ as that in a two-phase flow. This near-wall similarity between the bubbly flow and the single-phase water flow validate the fact that the limiting condition of the former one is one of the latter.

4.3.2. Bubble size effect on internal flow structure. Both figures 9 and 10 also present the data under two different nozzle jet conditions to change the bubble size at the entrance of the test section. Generally, the higher the nozzle jet velocity, the smaller are the bubbles generated. This effect is more pronounced when injecting bubbles into the low liquid flow condition. In order to explain the influences of bubble size on the wall shear stress more specifically, a typical phase distribution result of void fraction, bubble size and bubble frequency obtained previously (Liu 1993) is presented in figure 11. It can be seen that with a low nozzle jet ($J_j = 1.0$ m/s, open symbols), the profiles of bubble diameter and bubble frequency change from nearly uniform to parabolic as the gas velocity increased. By further increasing the nozzle jet velocity to a higher value ($J_j = 4.0$ m/s, solid symbols), the bubble size decreased drastically and bubbles were distributed more uniformly across the channel for the high J_G condition. Large numbers of these small bubbles tend to migrate toward the channel wall, resulting in a very sharp peak of void fraction and bubble frequency profiles near the wall. As observed in figures 9 and 10, these wall concentrated bubbles will increase the bubble–wall interaction resulting in higher values of mean and fluctuations of the wall shear stress. Spectral analysis of the temporal fluctuations as discussed earlier also support this result.

4.3.3. Bubble size effect on wall shear stress. A more complete data to illustrate the bubble size effect are presented in figure 12. It can be seen that under each fixed phasic flow rates condition, both the mean and its turbulent intensity of the wall shear stress in bubbly flow regime are generally increased with nozzle jet velocity. At high liquid velocity condition (such as $J_L = 3.0$ m/s), the mean wall shear stress and its fluctuations are almost independent of the jet velocities. Similar phenomenon also can be observed from figures 9 and 10. The reason is that the higher the mean liquid velocity, the smaller is the influence of nozzle jet on bubble size distribution. Most of these small bubbles with almost the uniform size tend to migrate toward the wall resulting in a high value of the mean wall shear stress and its fluctuations. However, as mentioned earlier, at the lower liquid flow rate condition the flow structure is more sensitive to the bubble size change, especially for the higher gas flow rate conditions. From figure 11(b), it is clearly indicated that the sizes of bubbles are drastically changed in the core region of the pipe flow, but has very limited difference in the vicinity of the wall. Apparently, the essential difference in each flow condition is the bubble number density near the wall; that is, the higher the nozzle liquid jet velocity, the larger are the number of these small bubbles concentrated at the wall region. It is likely that this highly concentrated bubbles will increase the collision rate between the bubble and the wall, thus promote the mean wall shear stress and its turbulent intensity. This high frequency of small bubbles closed to the wall causing an enhancement effect on wall shear stress also was confirmed by Marie *et al.* (1991).

However, in contrast to the above mentioned tendency shown in figure 12(a), under the conditions of $J_L = 1.0$ m/s and $J_G = 0.4$ m/s, the lower the jet speeds, the higher the wall shear stress fluctuations are found. Similar phenomenon also was found in $J_L = 2.0$ m/s and $J_G = 0.4$ m/s. The reason is that under these high gas fluxes and/or low liquid fluxes conditions, the variation of J_j from high to low will change the flow regime from bubbly flow to bubble–slug transition (or turbulent churn) flow as observed from the measuring station. This somewhat unstable flow regime generally persists a high turbulent shear fluctuations which also was observed by Nakoryakov *et al.* (1981).

5. COMPARISON BETWEEN EXPERIMENTS AND PREDICTIONS

The wall shear stress data obtained in this study are extensively compared with the prediction of the existing correlations or models in bubbly flow, such as Armand and Nevstrueva (1950), Herringe and Davis (1978), Beyerlein *et al.* (1985), Marie (1987), and Sato *et al.* (1981). Details of the equations are listed in table 3. The limit data available in the literature summarized by Sato *et al.* (1981) are also included. According to the published data and the correlations, there are two typical formats to illustrate the dependency of the relative wall shear stress on the

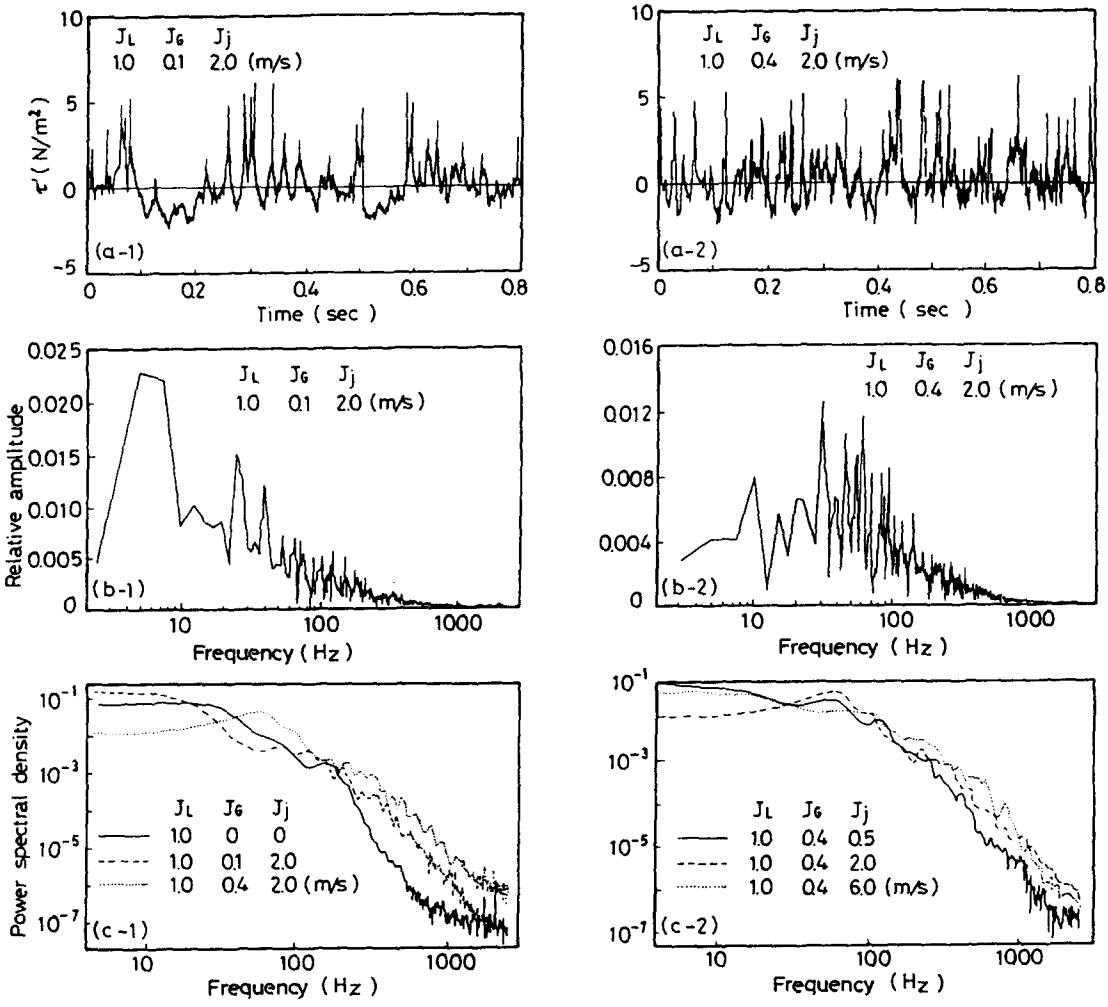

Figure 8. Statistical characteristics of wall shear stress fluctuations: (a) time history; (b) frequency spectrum; and (c) power spectral density.

two-phase flow parameters, namely the $\overline{\tau_w}/\overline{\tau_{wo}}(\beta)$ and the $\overline{\tau_w}/\overline{\tau_{wo}}(\langle\epsilon\rangle)$. As mentioned, $\overline{\tau_{wo}}$ represents the single-phase wall shear stress in which the water flow would be exerted by the bulk velocity of $J_L/(1-\langle\epsilon\rangle)$ as that in a two-phase flow. β is the volumetric gas flow rate ratio, defined by $J_G/(J_L+J_G)$.

Figure 13 presents the typical comparison results in the relation of $\overline{\tau_w}/\overline{\tau_{wo}}(\beta)$, while figures 14 and 15 present the results of $\tau_w/\tau_{wo}(\langle\epsilon\rangle)$ and $\tau_w/\tau_{wo}(\epsilon_{pk})$, respectively, The complete data of the present work under systematic test conditions and their predictions are listed in table 1. In this table, the value and position of the peaking void fraction are also provided for comparison with the Marie's model. The published data summarized by Sato *et al.* (1981) with additional predictions are listed in table 2. Due to unavailability of the corresponding single phase wall shear stress data, the values of $\overline{\tau_{wo}}$ in table 2 are calculated from [3].

5.1. Comparison with the relation of $\overline{\tau_w}/\overline{\tau_{wo}}(\beta)$

It can be seen from figure 13 that under the same water flow rate, the relation of $\overline{\tau_w}/\overline{\tau_{wo}}(\beta)$ strongly depends on bubble size and it is not unique. Nakoryakov *et al.* (1981) have observed that the flow in a bubbly regime at $J_L \leqslant 1$ m/s being that of the hysteresis type and the existence of

two stable bubbly flow regimes is possible. The data in the present study clearly indicate that the existence of more than two stable bubbly flow regimes under the identical gross flow condition (J_L and β) is validated. Besides, the present study found that this phenomenon is not limited to occur at $J_L \leqslant 1$ m/s. As mentioned, the higher the water jet in generating the small bubbles, the higher is the relative wall shear stress. This effect is decreased as the water velocity increased. The data of Nakoryakov *et al.* (1981) at $J_L = 1.06$ m/s and 2.05 m/s and of Sato *et al.* (1975, 1981) and Sekoguchi and Fukui (1975) at $J_L = 1.0$ m/s are also included in figure 13. One observed that the data of Sato and Sekoguchi fall in the range of the present data, which are consistent with the trend of bubble size effect as compared in table 1. It is also found that a big deviation was obtained from those of the Nakoryakov data at $J_L = 1.0$ m/s. The reason is not clear at this time. From the comparison of the present data as listed in table 1, with Armand and Nevstrueva's predictions, it can be seen that a constant value of the relative wall shear stress versus β fail to reflect the real physics, although the prediction in some cases give a good estimation.

5.2. *Comparison with the relation of* $\overline{\tau_w}/\overline{\tau_{wo}}(\langle\epsilon\rangle)$

Figure 14 gives the comparison of $\overline{\tau_w}/\overline{\tau_{wo}}(\langle\epsilon\rangle)$ predicted by Marie (1987), Beyerlein *et al.* (1985), and Herringe and Davis (1978) with the same set of data of Sato *et al.* and Sekoguchi as in figure 13. From figure 14(a), it is found that the lower the J_L the wider is the range of τ_w/τ_{wo} distributed over a narrow domain of $\langle\epsilon\rangle$. This phenomenon is more pronounced in the high J_G conditions. In contrast to the high J_L condition, such as $J_L = 3.0$ m/s, the above-mentioned phenomenon almost disappeared and the result was well predicted by both the Marie and the Herringe and Davis correlations. Figure 14(b) indicated that the predictions made by Beyerlein *et al.* are always lower than those of Herringe and Davis' results. The present data for the case of core peaking void distribution conditions are specified by solid symbols in figures 14(a) and 15(a), which are lower than those in the wall peaking data obtained by only increasing the J_j. Generally, the relatively high void fraction near the wall caused higher values of τ_w/τ_{wo}. In contrast, the higher the center void peaking profile, the lower is the two-phase wall shear stress which finally reach an equivalent

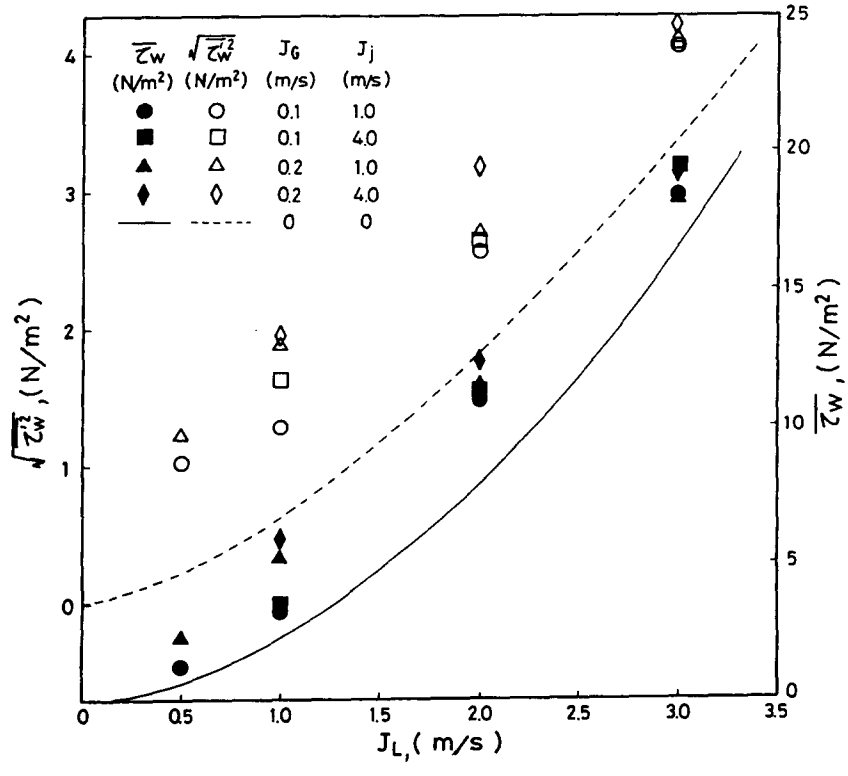

Figure 9. Superficial liquid velocity effect on the mean and turbulent intensity of wall shear stress.

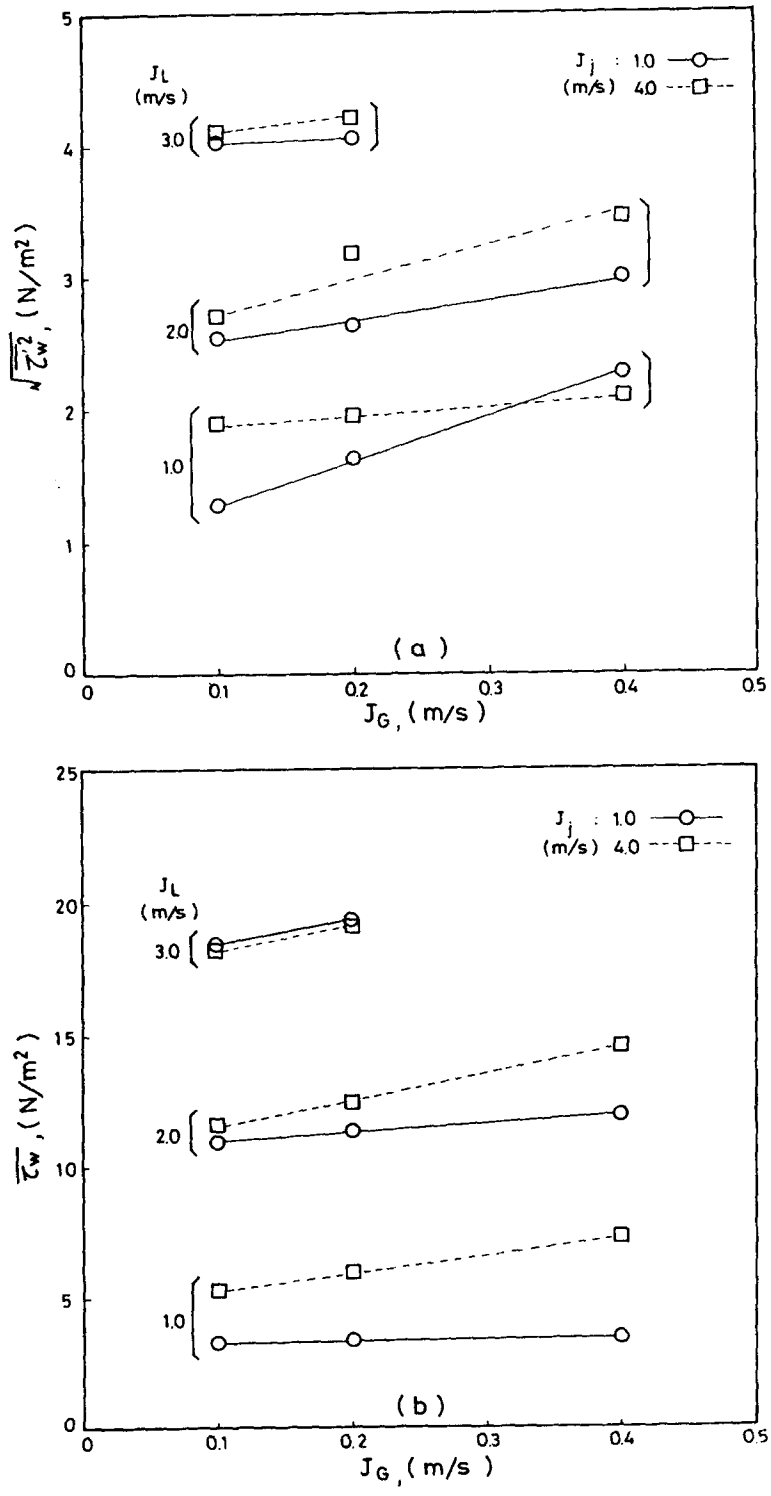

Figure 10. Superficial gas velocity effect on the mean and turbulent intensity of wall shear stress.

single-phase value. This phenomenon also was confirmed theoretically by Sato *et al.* (1981) from six different tentatively postulated void fraction profiles under the same gross flow condition. Recently, Marie *et al.* (1991) investigated the effects of bubbles on both the turbulent and the kinematic structures of a boundary layer on a flat plate. They also found that the wall shear stress

increases with the magnitude of the void fraction peak in the wall region. Figure 14(b) illustrates more clearly the above-mentioned effect related to the variation of the void fraction profile made by only changing the water jet velocities. From this figure, the non-uniqueness of the relation $\tau_w/\tau_{wo}(\langle\epsilon\rangle)$ is noted again. In addition, the two lowest data appeared in figure 14(a) are taken under the flow condition of bubbly–slug transition regime, as mentioned in section 4.3.3., where the effect of near-wall reverse liquid jet may be the reason that causes the two-phase wall shear stress to be lower than the equivalent single-phase one. It is also noted that the data of Sato and Sekoguchi at $J_L = 1.0$ m/s lie within the data range of the present study under the different values of J_j conditions due to the difference in bubble sizes as shown in table 2.

5.3. *Comparison with the relation of* $\overline{\tau_w}/\overline{\tau_{wo}}(\epsilon_{pk})$

Figure 15 gives the comparison of $\overline{\tau_w}/\overline{\tau_{wo}}(\epsilon_{pk})$ predicted by Marie (1987) with the present data. It should be noted from figure 15(a) that the prediction of Marie's model is highly improved as compared with the present data in the cases of the lower wall void peaking conditions, but a big deviation is still observed for the higher wall void peaking conditions. Figure 15(b) further

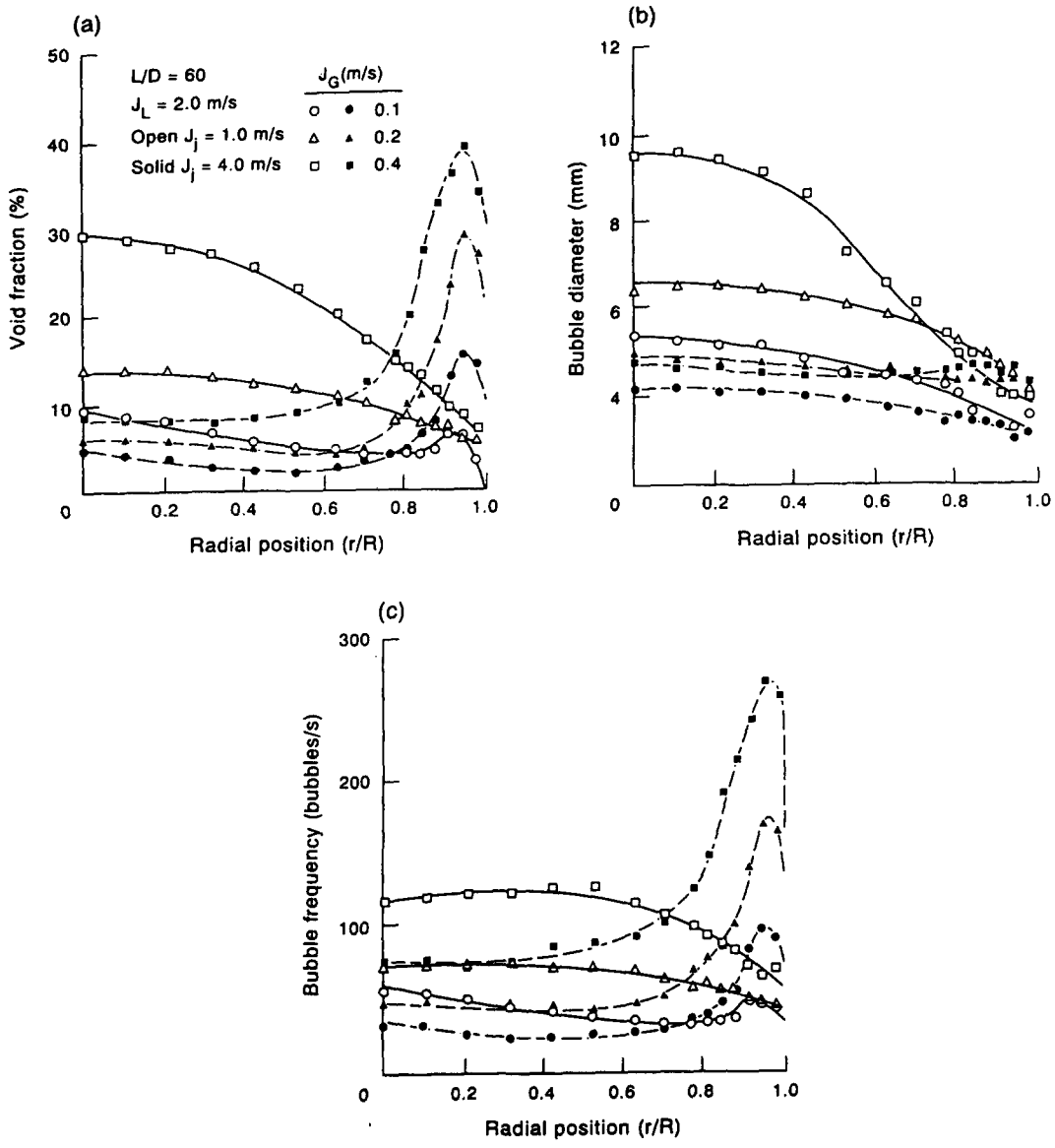

Figure 11. Typical phase distribution results of (a) void fraction, (b) bubble size, and (c) bubble frequency.

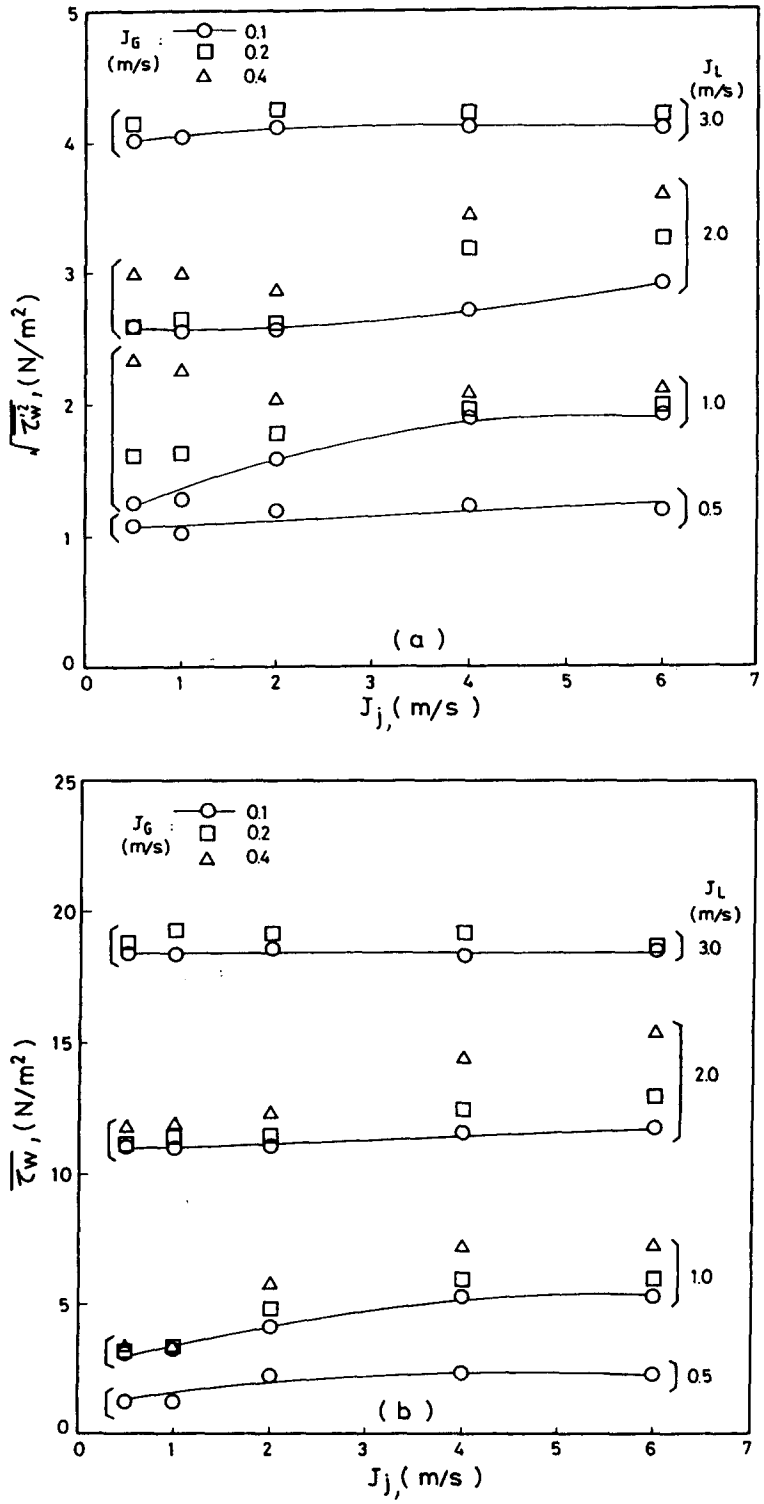

Figure 12. Bubble size effect on the mean and turbulent intensity of the wall shear stress.

illustrates the effect related to the peaking void fraction by only changing the water jet velocity. It is interesting to note that the two sets of the present data (at $J_L = 1.0$ m/s, $J_j = 2.0$ m/s and at $J_L = 2.0$ m/s, $J_j = 6.0$ m/s) all lie closely to the prediction of Marie's model. However, it is still unsatisfactory to predict two other bubbling conditions.

Table 2. Comparison of the published two-phase wall shear stress data with correlations

References	Condition J_L (m/s)	J_G (m/s)	$\langle d_b \rangle$ (mm)	$\langle \epsilon \rangle$ (%)	D (mm)	β (%)	Measured data $\overline{\tau_{wo}}$ (Pa)	$\overline{\tau_w}$ (Pa)	R_{exp}	R_{Mav}	R_{HDv}	R_{ANv}	Model prediction R_{Bav}	$\overline{\tau_{Sw}}$ (Pa)	R_{SBav}
	0.50	0.056	4.4	7.1		10.1	0.99	1.65	1.66	1.19	1.02	1.14	1.05	1.24	1.25
	0.50	0.105	4.8	13.1		17.4	1.12	2.14	1.92	1.35	1.04	1.27	1.06	1.47	1.31
Sato (1981)	0.70	0.104	4.5	10.2	26.0	12.9	1.90	3.09	1.62	1.27	1.03	1.19	1.06	2.51	1.32
	0.70	0.244	5.6	22.2		25.9	2.45	4.43	1.81	1.49	1.09	1.45	1.09	3.74	1.53
	1.00	0.104	4.0	8.3		9.4	3.44	4.95	1.44	1.03	1.02	1.13	1.04	5.11	1.49
	1.00	0.243	4.6	17.3		19.6	4.13	6.46	1.56	1.14	1.06	1.31	1.07	6.46	1.56
Malnes (1966)	1.50	0.643	3.0	26.0	46.0	30.0	9.14	9.52	1.04	1.25	1.11	1.55	1.06	14.28	1.56
Sato (1975)	1.00	0.207	3.5	11.7	34.8	17.1	3.44	5.69	1.65	1.15	1.04	1.27	1.05	5.86	1.70
Sekoguchi (1975)	1.00	0.101	3.4	6.9	35.4	9.2	3.12	3.64	1.17	1.08	1.02	1.13	1.03	3.32	1.06

The non-uniqueness of the relationships among $\overline{\tau_w}/\overline{\tau_{wo}}(\beta)$, $\overline{\tau_w}/\overline{\tau_{wo}}(\langle\epsilon\rangle)$ and $\overline{\tau_w}/\overline{\tau_{wo}}(\epsilon_{pk})$ is proved experimentally due to the existence of different flow structures under the same gross flow and the same geometry condition. It should be noted that in the present study the only parameter affecting the flow structure in two-phase bubbly flow is the diameter of bubbles generated at inlet. Due to no previous wall shear stress data accounted for the change in initial bubble size condition and the related detail flow structure at the measuring station, none of the correlation can handle the present results very well.

5.4. *Comparison with the Sato* et al. *model*

The present wall shear stress data are compared with the prediction of the theoretical model proposed by Sato, Sadatomi and Sekoguchi (1981) using the fully developed axial momentum equation in a vertical bubbly flow. In Sato *et al.* model, wall shear stress is assumed to be proportional to the superposition of both ε' and ε'', where ε' is the eddy diffusivity due to wall-induced turbulence and ε'' is due to bubble agitation. An empirical expression for the local bubble size d_b was recommended to account for the effect of bubble size distribution on ε''. Based on this model, the liquid velocity profile can be numerically calculated by iteration for a given input void fraction profile. In the iteration scheme, the wall shear stress is the only adjustable parameter provided the agreement between predicted and measured mass flow rate was satisfied. Before applying this model to the present test conditions, a self-written computer program was extensively validated with Sato *et al.* (1981) predictions presented in their paper with sufficient accuracy. Figure 16 gives a comparison of the Sato *et al.* model prediction on the distribution of flow parameters in a typical bubbly flow with the present work. The accuracy of the wall shear stress predictions was found to be strongly dependent on the number of grid points along the radial direction. Their sensitivity was well-examined by interpolating the measured void fraction data. Generally, less than 1% error of the wall shear stress can be expected as the selected grid number was larger than 10^4.

The results of wall shear stress prediction for all of the 45 different bubbling conditions under which the input void fraction profile was interpolated into 2×10^4 equally-spaced grids are listed

Table 3. Previous correlations and models

Authors	Correlation or model
Armand and Nevstrueva (1950)	$\overline{\tau_w}/\overline{\tau_{wo}} = (1 - 0.833\beta)^{-1.53}$
Herringe and Davis (1978)	$\overline{\tau_w}/\overline{\tau_{wo}} = 1 + 0.22\langle\epsilon\rangle + 0.82\langle\epsilon\rangle^2$
Beyerlein *et al.* (1985)	$\overline{\tau_w} = 0.0791 \cdot \mathrm{R}_e^{-1/4} \cdot \rho_L \left[\dfrac{J_L^2}{2(1-\langle\epsilon\rangle)^2}\right]$
Marie (1987)	$\overline{\tau_w}/\overline{\tau_{wo}} = 1 + \dfrac{10}{3(1-\langle\epsilon\rangle)}\sqrt{1.1\langle\epsilon\rangle(1-\langle\epsilon\rangle)}\,\dfrac{U_x}{J_L}$
Sato *et al.* (1981)	$\tau/\overline{\tau_w} = (1 - B \cdot \int_0^1 \epsilon \cdot r^* \mathrm{d}r^*) \cdot r^* + B/r^* \int_0^{r^*} \epsilon \cdot r^* \mathrm{d}r^*$

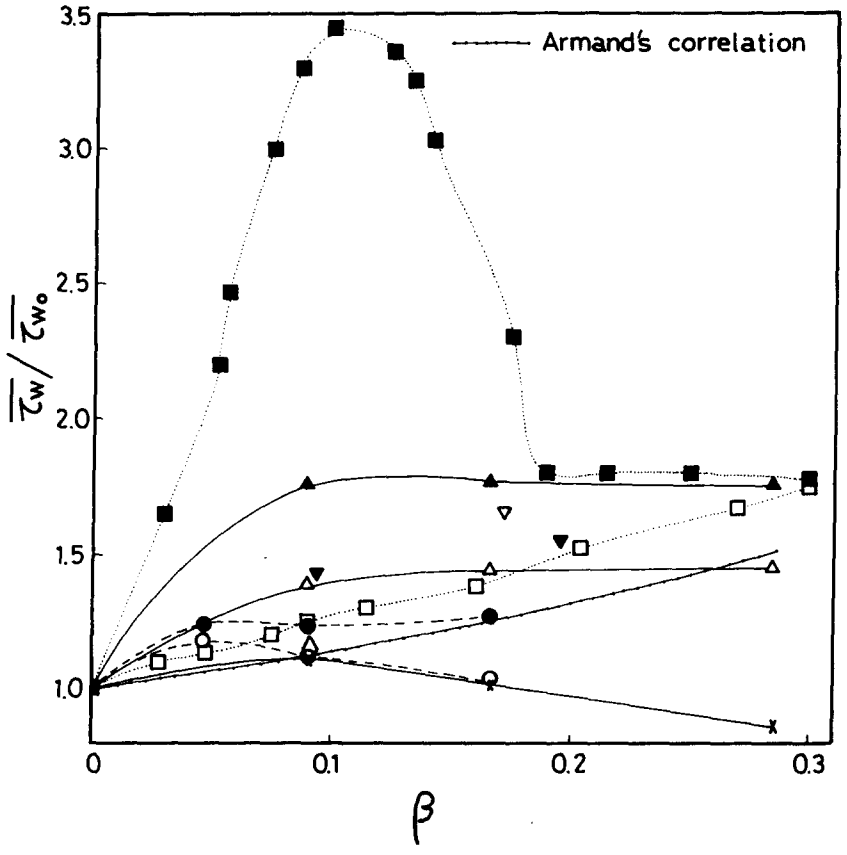

Figure 13. Comparison of the $\overline{\tau_w}/\overline{\tau_{wo}}(\beta)$ data with Armand and Nevstrueva's prediction.

in table 1. The final result was obtained as the calculated mass flow rate converged to the measured one with absolute error smaller than 5×10^{-7} between iterations. It can be seen that Sato *et al.* model well-predicted the bubble size effect, namely, a higher value of wall shear stress appears in the case of relatively high void fraction near the wall. The predicted values of τ_{Swo} based on the single-phase water flows of $J_L/(1 - \langle\epsilon\rangle)$ are also in good agreement with the measured data τ_{wo}. However, the model generally over-predicted the wall shear stress in two-phase bubbly flow except for the case of $J_L = 0.5$ m/s. In this study, two ways were utilized to calculate ε'' as a function of bubble sizes. In table 1, R_{SBav} and R_{SB} defined as the predicted ratios of the two-phase wall shear stress to that of the τ_{Swo} obtained from the above mentioned empirical expression and the measured bubble size distribution d_b, respectively. It can be seen that the predicted values of R_{SB} are consistent with that of R_{SBav} at $J_L = 3$ m/s. At lower J_L conditions, however, rather higher values of R_{SB} were predicted.

6. CONCLUSIONS

From the above discussion, one can conclude that the wall shear stress and its turbulent fluctuations in bubbly flow regime are indeed, strongly dependent on the flow structure near the wall. The shear stress is primarily due to the predominant role of multi-peak large-scale low-frequency wave components. However, the interaction between the wall concentrated bubbles and the thin liquid film proximity to the wall outweigh the high-frequency small-scale wave components, promoted both the mean and fluctuation intensity of the wall shear stress. The new data accounted for the parametric effects of the bubble size and the two phases flow rates on wall shear stress are reported. Among these effects in bubbly flow, both of the mean liquid velocity and the wall concentrated bubbles are found to be the dominant parameters that influence both the magnitude and the fluctuation intensity of the wall shear stress. Due to no obvious existing wall

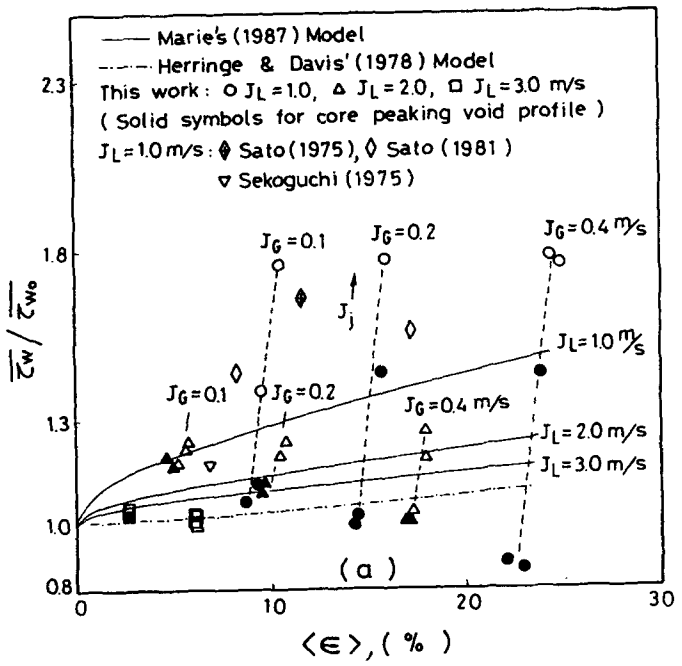

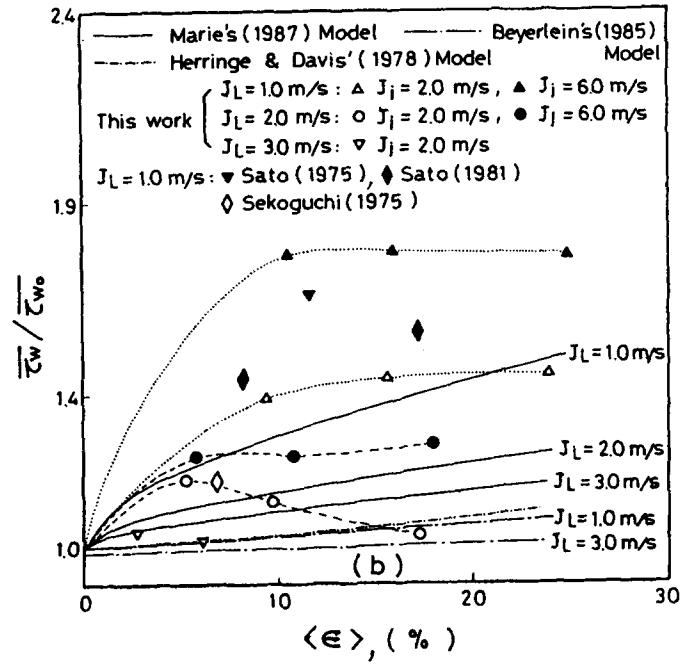

Figure 14. Comparison of the $\overline{\tau_w}/\overline{\tau_{wo}}(\langle\epsilon\rangle)$ data with Herringe and Davis', Beyerlein's and Marie's predictions of (a) superficial liquid flow rate effect, and (b) initial bubble size effect.

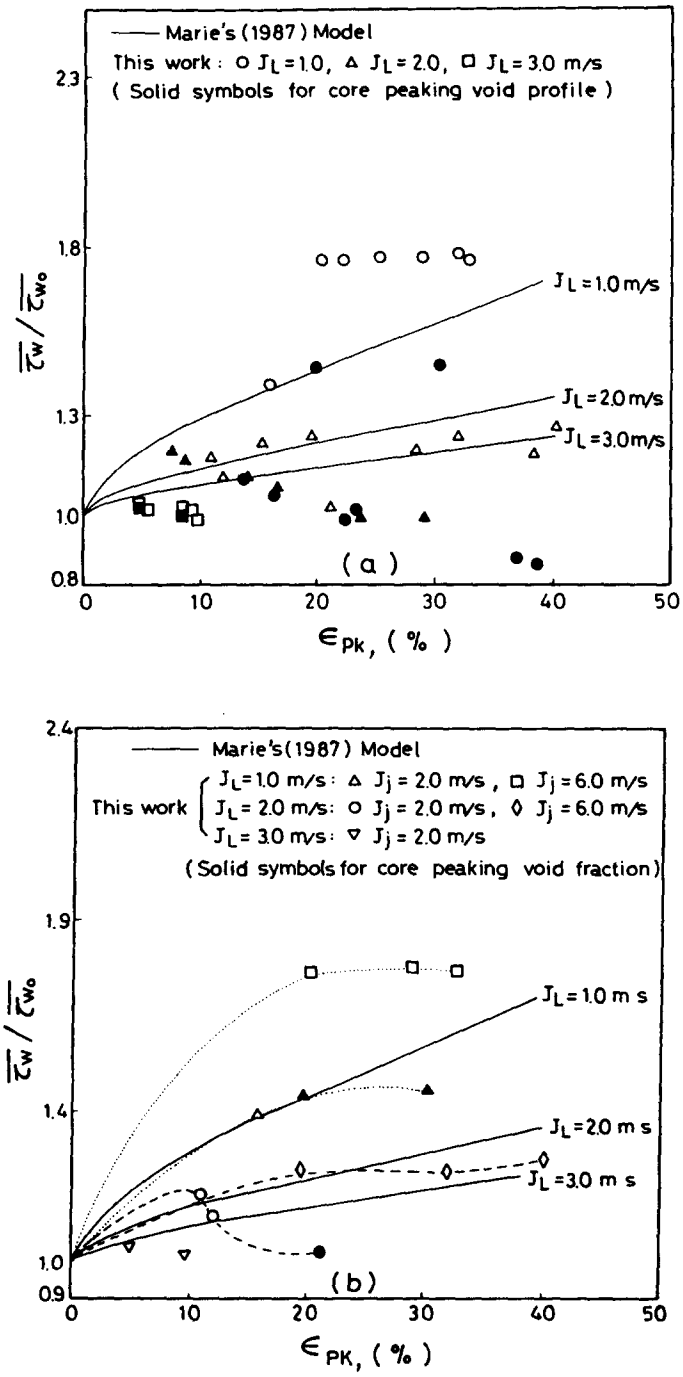

Figure 15. Comparison of the $\overline{\tau_w}/\overline{\tau_{wo}}(\epsilon_{pk})$ data with Marie's prediction of (a) superficial liquid flow rate effect, and (b) initial bubble size effect.

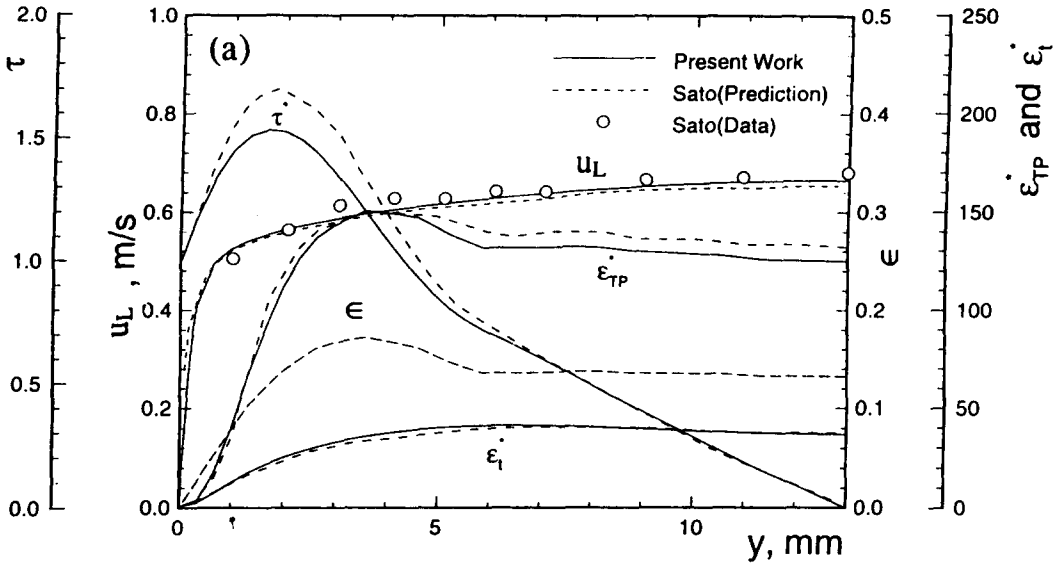

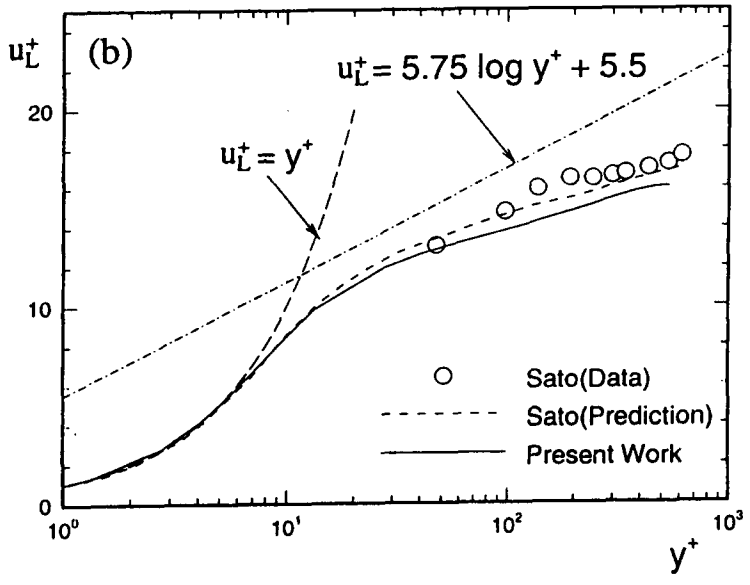

Figure 16. Comparison of the Sato *et al.* model prediction on (a) the distribution of flow parameters and (b) the logarithmic velocity distribution in a typical bubbly flow with the present work.

shear stress data and models were accounted for the change in bubble size systematically, the present data thus may serve as a relatively complete comparative basis for the development of theoretical models.

Acknowledgements—The author wishes to express his gratitude to Mr W. T. Hong and Mr F. Z. Yeh for their help during the experiments.

REFERENCES

Armand, A. A. and Nevstrueva, E. I. (1950) Investigation of mechanism of two-phase mixture transport in a vertical tube. *Izv. VTI* **2,** 1–8.

Avdeev, A. A. (1984) Turbulent flow hydrodynamics of a bubbly two-phase mixture. *J. of Engng Physics* 536–544.

Beyerlein, S. W., Cossmann, R. K. and Richter, H. J. (1985) Prediction of bubble concentration profiles in vertical turbulent two-phase flow. *Int. J. Multiphase Flow* **11,** 629–641.

Davis, M. R. (1974) The determination of wall friction for vertical and horizontal two-phase bubbly flows. *J. Fluids Engng* 173–179.

Herringe, R. A. and Davis, M. R. (1976) Structure development of gas–liquid mixture flows. *J. Fluid Mech.* **73,** 97–123.

Herringe, R. A. and Davis, M. R. (1978) Flow structure and distribution effects in gas–liquid mixture flows. *Int. J. Multiphase Flow* **4,** 461–486.

Kariyasaki, A. (1985) Behaviour of a gas bubble in a liquid flow with a linear velocity profile. In *Proc. 7th Two-phase Flow Symposium of Japan.*

Lahey, R. T., Jr (1988) Phase distribution and phase separation phenomena in two-phase flows. In *Proc. Int. Topical Meeting on Nuclear Power Plant Thermalhydraulics and Operations*, Seoul, Korea.

Liu, T. J. (1991) The effect of bubble size on void fraction distribution in a vertical channel. In *Proc. Int. Conf. on Multiphase Flows '91*, Tsukuba, Japan, pp. 453–457.

Liu, T. J. and Bankoff, S. G. (1993a) Structure of air–water bubbly flow in a vertical pipe: I. liquid mean velocity and turbulence measurements. *Int. J. Heat Mass Transfer* **36,** 1049–1060.

Liu, T. J. and Bankoff, S. G. (1993b) Structure of air–water bubbly flow in a vertical pipe: II. Void fraction, bubble velocity and bubble size distribution. *Int. J. Heat Mass Transfer* **36,** 1061–1072.

Liu, T. J. (1993) Bubble size and entrance length effects on void development in a vertical channel. *Int. J. Multiphase Flow* **19,** 99–113.

Liu, T. J. (1994) Measurements of local interfacial area concentration in two-phase bubbly flow. In *Proc. of the 4th Int. Topical Meeting on Nuclear Thermal Hydraulics, Operations and Safety*, 6–8 April, Taipei, Taiwan, 8-B-1-6.

Marie, J. L. (1987) Modelling of the skin friction and heat transfer in turbulent two-component bubbly flows in pipes. *Int. J. Multiphase Flow* **13,** 309–325.

Marie, J. L., Moursali, E. and Lance M. (1991) A first investigation of a bubbly boundary layer on a flat plate: phase distribution and wall shear stress measurements. In *Proc. Turbulence Modification in Multiphase Flows*, ASME FED-Vol. 110, pp. 75–80.

Marple, S. L., Jr (1987) *Digital Spectral Analysis with Applications*. Prentice-Hall, New Jersey.

Martin C. J. (1984) The non-intrusive measurement of wall shear stress and velocity profiles in vertical annular two phase flow. In *Proc. New Experimental Techniques in Heat Transfer*. ASME, pp. 47–54.

Matsui, G. (1988) Characteristic structure of upward bubble flow under the same flow rate conditions. In *Proc. Japan–U.S. Seminar on Two-phase Flow Dynamics*, Ohtsu, Japan, E.2-1–E.2-10.

Moursali, E., Marie, J. L. and Bataille, J. (1995) An upward turbulent bubbly boundary layer along a vertical flat plate. *Int. J. Multiphase Flow* **21,** 107–117.

Nakoryakov, V. K., Kashinsky, O. N., Burdukov, A. P. and Odnoral, V. P. (1981) Local characteristics of upward gas–liquid flows. *Int. J. Multiphase Flow* **7,** 63–81.

Sato, Y., Sadatomi, M. and Sekoguchi, K. (1981a) Momentum and heat transfer in two-phase bubble flow–I: theory. *Int. J. Multiphase Flow* **7,** 167–177.

Sato, Y., Sadatomi, M. and Sekoguchi, K. (1981b) Momentum and heat transfer in two-phase bubble flow-II: a comparison between experimental data and theoretical calculations. *Int. J. Multiphase Flow* **7**, 179–190.

Sato, Y. and Sekoguchi, K. (1975) Liquid velocity distribution in two-phase bubble flow. *Int. J. Multiphase Flow* **2**, 79–95.

Sekoguchi, K., Sato, Y. and Honda, T. (1974) An experimental investigation on bubble flow (first report). *Trans. Japan Soc. Mech. Engrs* **40**, 1395–1403 (in Japanese).

Sekoguchi, K. and Fukui, H. (1975) Investigation into statistical characteristics of bubbles in two-phase flow—experimental results for velocity and void fraction distributions. *Trans. Japan Soc. Mech. Engrs* **758-2**, 90–93.

Sekoguchi K., Fukui, H. and Sato, Y. (1979) Flow characteristics and heat transfer in vertical bubble flow. In *Proc. Japan–U.S. Seminar on Two-phase Flow Dynamics*, Kansai, Japan, pp. 59–74.

Serizawa, A., Kataoka, I. and Michiyoshi, I. (1975) Turbulence structure of air–water bubbly flow. *Int. J. Multiphase Flow* **2**, 221–246.

Serizawa, A. and Kataoka, I. (1987) Phase distribution in two-phase bubbly flow. *Proc. of the ICHMT Seminar on Transient Phenomena in Multiphase Flow*, Dubrovnik, Yugoslavia, pp. 179–224.

Serizawa, A., Kataoka, I., Zun, I. and Michiyoshi, I. (1988) Bubble size effect on phase distribution. In *Proc. Japan–U.S. Semin. on Two-phase Flow Dynamics*, Ohtsu, Japan, pp. 15–20.

Serizawa, A., Kataoka, I., Gofuku, A., Takahashi, O. and Kawara, Z. (1991) Effect of initial bubble size on bubbly flow structure. In *Proc. Int. Conf. on Multiphase Flows* '91, Tsukuba, Japan, pp. 547–550.

Valukina, N. V., Koz'menko, B. K. and Kashinskii, O. N. (1979) Characteristics of a flow of monodisperse gas–liquid mixture in a vertical tube. *Inzhenerno-Rizicheskii Zhurnal* **36**, 695–699.

Whalley, P. B. and McQuillan, K. W. (1985) The development and use of a directional wall shear stress probe. In *Proc. 2nd Int. Conf. on Multiphase Flow*, London, pp. 317–327.

Zun, I. (1987) Transition from wall void peaking to core void peaking in turbulent bubbly flow. *Proc. of the ICHMT Seminar on Transient Phenomena in Multiphase Flow*, Dubrovnik, Yugoslavia, pp. 225–245.

Zun, I. and Malahovsky, A. (1982) The terminal properties of single gas bubbles. In *Proc. 3rd Chemical Engineering Congress*, Graz, pp. 112–119.